RESEARCH ARTICLE

Numerical Study of the Influence of Pressure on the Dynamics and Complex Bifurcation Processes of the Low-Pressure DC Glow Discharge

XITONG ZHAO
Department of Mathematics, College of Sciences, Shanghai University, Baoshan, Shanghai 200444, China
e-mail: Xitong_Zhao_Shu@163.com

ABSTRACT We study the dynamics and complex bifurcation processes of the low-pressure direct current (DC) argon glow discharge system on the basis of a spatially dependent model. In particular, a plasma fluid model based on the drift-diffusion approximation is established, and the Resistor-Capacitance (RC) external circuit is coupled into the model as a boundary condition. The bifurcation processes, which are characterized by the temporal evolution of the discharge voltage and current, are obtained by changing the control parameter, *i.e.*, the discharge pressure p. The results indicate an order-chaos-order transition due to changes in pressure, showing that increasing pressure can induce similar transitions in discharge modes as increasing the applied voltage U_0. The applied voltage is introduced as second parameter and a finite number of "bubbles" bifurcation structure is formed on some cross-sections of the two-parameter plane. It is suggested that the chaotic oscillations exist only under certain parameter range. Far from the certain parameter region, only periodic behaviors can be observed. The results can provide some guidance for plasma applications in practice.

I. INTRODUCTION

In recent years, there has been notable advancement in gas discharge plasma technology [1], [2], [3]. It has been observed by researchers that direct current (DC)-driven self-pulsing discharges induced by negative differential resistivity (NDR) can achieve higher transient power as well as plasma densities compared to steady-state discharges under equivalent average power conditions [4], [5]. In practical applications, depending on specific requirements, direct current-driven self-pulsing discharges may include various forms such as corona discharge, glow discharge, and plasma jet [6], [7], [8]. DC-driven self-pulsing discharges has been recognized for their potential in various fields, including sterilization [9], nitrogen fixation [10], and as sensors in medical treatments [11], respiratory monitoring [12], smoke detection [13], etc.

The associate editor coordinating the review of this manuscript and approving it for publication was Ludovico Minati.

However, most previous studies have focused on regular and repeatable self-pulsing discharge. Actually, it is necessary to keep the performance of the discharge device stable or controllable in industrial production as well as in daily lighting applications. Chaos may be undesirable for industrial applications where cycle-to-cycle reproducibility is important. However, in the treatment of cell-containing materials, including living tissues, using plasma technology, it may offer a novel approach to addressing major challenges in medicine such as drug resistance [14]. This has sparked a strong interest in studying the nonlinear dynamic behaviors in plasma and their impact on parameters.

As a highly nonlinear medium, there are a variety of nonlinear mechanisms and the interaction of the coupling among the nonlinear mechanisms due to the time scales within the gas discharge plasma spanning several orders of magnitude [15]. Thus, even in its simplest form, the DC glow discharge device exhibits numerous nonlinear phenomena. These include spatial nonlinear behaviors such

as self-organized patterns [16], [17], striations in the positive column region [18], [19], as well as temporal nonlinear behaviors such as period-doubling bifurcation, quasi-periodicity, chaos [20], [21], and more. Rafatov et al. developed a one-dimensional fluid model and demonstrated the existence of the period-doubling bifurcation route to chaos in semiconductor-gas nitrogen discharge systems by varying the applied voltage under the specified discharge parameters, and obtained a bifurcation diagram which is similar to the one-dimensional unimodal mapping [22]. Similar period-doubling bifurcation processes in other discharge systems has been reported in several other works, both in experiments and simulations [23], [24], [25]. However, for more general conditions, the dynamic behavior of the discharge system can be affected by changes in the internal discharge conditions in addition to the external electrical parameters. There are numerous works reporting the effect of discharge conditions on the nonlinear dynamic behaviors exhibited by gas discharge plasmas. For example, Ya Hong et al. investigated the nonlinear dynamic behaviors of a helium-air Dielectric Barrier Discharge (DBD) in the two-parameter plane by considering the influence of different impurity concentrations and the applied voltage. The results show that increasing the impurity concentration can significantly affect the nonlinear dynamic behavior, such as leading to the formation of multi-pulse discharges [26], [27]. Walsh et al. reported an experimental observation of the dynamic behavior of an atmospheric-pressure dielectric barrier plasma jet, which is reveal that the system could exhibit regimes of periodic, quasi-periodic and chaotic behaviors due to the influence of gas flow rate [14].

It is well known that pressure, as an essential parameter for gas discharges, can significantly influence the discharge characteristics such as plasma density distribution and current-voltage characteristics [28], [29], [30]. Most of the previous studies on the nonlinear dynamic behavior in plasma have focused on the atmospheric pressure dielectric barrier discharge structure. For low-pressure DC glow discharge, it remains unclear whether pressure significantly influences the nonlinear dynamic behavior of the discharge. Therefore, a more detailed analysis of the nonlinear dynamic behavior of DC glow discharge under different discharge pressures is needed. Since the gas discharge system involves complex physical and chemical reaction processes, numerical simulation is less time-consuming compared to experimental observation and can clearly help to further understand the plasma discharge process and the parameter dependence.

For this purpose, we establish a two-dimensional plasma fluid model and coupling an external circuit into the model as a boundary condition to investigate the influence of pressure on the nonlinear dynamic behavior of the argon DC glow discharge. The control parameters are chosen as the pressure p and the applied voltage U_0. It is found that a finite of ''bubbles'' is formed on some cross-sections of the two-parameter plane due to the finite period-doubling

bifurcation sequences and the corresponding remerging inverse bifurcation trees. The paper is organized as follows: After this introduction, the governing equations are given in Section II, the calculation results the discussion are presented in Section III and the conclusions obtained from the simulations are summarized in Section IV.

II. SIMULATION MODEL
A. GOVERNING EQUATIONS
In this work, a DC gas discharge system between two parallel electrodes in a long straight vacuum tube is considered. The length of the discharge tube is $L = 15$ cm, the electrode gap is $d = 7$ cm, and the radii of the discharge tube and the electrode are $R_0 = 1.25$ cm and $R_1 = 1.2$ cm. The electron configuration has been widely used in applications such as fluorescent lighting. Considering that the effect of diffusion of charged particles on the wall in a long narrow discharge tube could not be negligible [31], a two-dimensional plasma fluid model based on the drift-diffusion approximation is built instead of the typical one-dimensional model used to describe short-gap discharges such as DBD. Argon is chosen as the working gas and three species, namely, electrons, argon ions and metastable argon atoms are considered. The chemical reactions considered in this work are identical to those in [28], [31], [32], and [33] and are given in Table 1. The plasma fluid model includes continuity equations for both particles and electron energy, as well as Poisson's equation. The governing equations are as follows:

$$\frac{\partial n_k}{\partial t} + \nabla \cdot \mathbf{\Gamma}_k = S_k, \tag{1}$$

$$\frac{\partial n_\varepsilon}{\partial t} + \nabla \cdot \mathbf{\Gamma}_\varepsilon = -e\mathbf{\Gamma}_e\mathbf{E} + S_\varepsilon, \tag{2}$$

$$-\varepsilon_0 \nabla^2 \varphi = \sum_k q_k n_k, \mathbf{E} = -\nabla\varphi \tag{3}$$

where n_k and n_ϵ represent the particle density and the electron energy density, respectively. ∇ represent the Nabla operator. Subscripts k indicates the kth species (e, Ar^+, Ar_m). E and φ are the electric field and potential. ϵ_0 is the vacuum permittivity. S_k and S_ϵ represent the source terms of the particle and electron energy due to the collision reaction. Γ_k and Γ_ε represent the flux of particle and energy, respectively, and under the drift-diffusion approximation, they have the following forms,

$$\mathbf{\Gamma}_k = -\mu_k n_k \mathbf{E} - D_k \nabla n_k, \tag{4}$$

$$\mathbf{\Gamma}_\varepsilon = -\mu_\varepsilon n_\varepsilon \mathbf{E} - D_\varepsilon \nabla n_\varepsilon, \tag{5}$$

the relationship between electron density and electron energy density can be expressed as $n_\varepsilon = n_e\overline{\varepsilon}$, where $\overline{\varepsilon} = 3/2k_BT_e$ represents the mean electron energy. μ and D is the mobility and diffusion coefficient, respectively. For electron, μ_e and D_e are obtained from the following equations,

$$\mu_e = -\frac{2e}{m} \int_0^{+\infty} \frac{\varepsilon}{3v_{ea}} \sqrt{\varepsilon} \frac{\partial}{\partial \varepsilon} f_0(\varepsilon) d\varepsilon, \tag{6}$$

$$D_e = \frac{2e}{m} \int_0^{+\infty} \frac{\varepsilon}{3\nu_{ea}} \sqrt{\varepsilon} f_0(\varepsilon) d\varepsilon, \tag{7}$$

where ε is the kinetic energy of electron, ν_{ea} represents the momentum transfer frequency. $f_0(\varepsilon)$ is the electron energy distribution function, and is assumed to follow the Maxwell distribution in current model, which has been demonstrated as viable in other researchers' works. The relationship of the transport coefficient between electron and the electron energy satisfied $\mu_\varepsilon = 5/3\mu_e$ and $D_\varepsilon = 5/3D_e$.

According to the chemical reactions involved in the numerical model, the source terms S_k and S_ε are calculate by

$$S_e = S_i = k_2 n_0 n_e + k_5 n_m n_e + k_6 n_0 n_m, \tag{8}$$

$$S_m = k_3 n_0 n_e - k_4 n_e n_m - k_5 n_e n_m - 2k_6 n_m^2 - k_7 n_0 n_m, \tag{9}$$

$$S_\varepsilon = -3/2\delta\nu_{ea} n_e k_B(T_e - T_g) + k_2 n_0 n_e \Delta E_2$$
$$+ k_3 n_0 n_e \Delta E_3 + k_4 n_m n_e \Delta E_4 + k_5 n_m n_e \Delta E_5, \tag{10}$$

where n_0 is the neutral argon density, $\delta = 2m_e/m_g$, $T_g = 300K$ is the background gas temperature, and k_n is the rate constant corresponding to the n-th reaction, and the relationship between the rate constant and the cross section is

$$k_n = \int_0^\infty \sigma_n(\varepsilon) \nu(\varepsilon) \sqrt{\varepsilon} f_0(\varepsilon) d\varepsilon. \tag{11}$$

B. BOUNDARY CONDITIONS

The normal flux of electrons and electron energy at the boundary are given by

$$\boldsymbol{n} \cdot \boldsymbol{\Gamma}_e = \frac{1-r_e}{1+r_e} \frac{1}{2} \nu_{e,th} n_e + n_e \mu_e (\boldsymbol{E} \cdot \boldsymbol{n})) + \sum_i \gamma_i (\boldsymbol{\Gamma}_i \cdot \boldsymbol{n}) \tag{12}$$

$$\boldsymbol{n} \cdot \boldsymbol{\Gamma}_\varepsilon = \frac{1-r_e}{1+r_e} \frac{5}{6} \nu_{e,th} n_e + n_\varepsilon \mu_\varepsilon (\boldsymbol{E} \cdot \boldsymbol{n})) + \sum_i \gamma_i \overline{\varepsilon_i} (\boldsymbol{\Gamma}_i \cdot \boldsymbol{n}) \tag{13}$$

where $\boldsymbol{n}$ is the unit vector of outer normal direction at the boundary; $\nu_j = \sqrt{8k_B T_j/\pi m_j} (j = e, i, m)$ represents the thermal velocity; $\gamma = 0.2$ is secondary electron emission coefficient; $\overline{\varepsilon_i}$ is the mean energy of secondary electrons. For argon ions, the boundary condition is as follows,

$$\boldsymbol{n} \cdot \boldsymbol{\Gamma}_i = 1/4 n_i \nu_i - \alpha n_i \mu_i (\boldsymbol{n} \cdot \boldsymbol{E}), \tag{14}$$

where the coefficient $\alpha = 1$ when $(\boldsymbol{n} \cdot \boldsymbol{E}) > 0$, otherwise $\alpha = 0$. For excited atoms, the boundary condition is given by:

$$\boldsymbol{n} \cdot \boldsymbol{\Gamma}_m = 1/4 n_m \nu_m. \tag{15}$$

For the electric potential, the Resistor-Capacitance (RC) external circuit is coupled into the model as a boundary condition. At the cathode, the potential is set to $\varphi = 0$, while at the anode, the potential is set to $\varphi = U$, which is satisfied by,

$$\frac{dU}{dt} + \frac{1}{C}(I - \frac{U_0 - U}{R}) = 0, \tag{16}$$

where U_0 and I represent the applied voltage and total current, respectively. The ballast resistance is set to $R = 10^6\ \Omega$, and the capacitance is set to $C = 10$ pF. The initial anode potential is set to $U = U_0$, and the initial distribution of electron density, argon ion density, and electron temperature are set to $n_e(r, z, t = 0) = n_i(r, z, t = 0) = 1.0 \times 10^{13} m^{-3}$, $T_e(r, z, t = 0) = 2$ eV, respectively. Heat generated by Joule heating has a negligible impact on circuit performance and can be safely disregarded due to the lower average power of the discharge system under the subnormal glow discharge regime [36], [37], which preclude the formation of transversal spatial patterns [38], [39], i.e. we are studying spatially homogeneous temporal oscillations. The model was realized in COMSOL Multiphysics software (COMSOL, Inc., Burlington, MA, USA) based on the finite-element method, and the implicit time-stepping backward differentiation formula (BDF) method is employed. The solver's time steps are dictated by the algorithm, with an adaptive size being selected according to the local error estimates.

III. RESULTS AND DISCUSSION

The most obvious consequence of varying pressure is the change in the current-voltage characteristics of the system. Fig.1 shows the CVCs curve calculated at different pressures. The calculated pressures are set at $p = 20$ Pa ~ 80 Pa with an interval of 15 Pa. It can be seen from the figure that the N-type CVC can be roughly divided into the following regions: When the current is less than about 10^{-6} A, the system is in the Townsend discharge or dark discharge regime, characterized by a positive slope in the CVC; Subsequently, a notable negative slope is observed when the current exceeds 10^{-6} A, indicating that the breakdown process occurs and the system transitions from the Townsend discharge regime to the glow discharge regime. The transition regime is known as the subnormal glow discharge regime. From Fig.1, it is evident that the breakdown voltage decreases monotonically with increasing pressure, indicating that the discharge conditions lie on the left side of the Paschen curve, i.e., $pd > pd_{min}$, where pd_{min} corresponds to the minimum of the Paschen curve. Arslanbekov et al. demonstrated that when the discharge device is operating in the subnormal discharge regime, the plasma may exhibit time-domain oscillations as a result of the presence of NDR [35]. The majority of previous studies have suggested that the instability in question manifests exclusively on the right side of the Paschen curve [22]. In this work, to the best of our knowledge, numerical evidence is presented for the first time demonstrating the existence of self-sustained oscillations and even chaotic oscillations on the left side of the Paschen curve.

Subsequently, the pressure is chosen as the control parameter, with the applied voltage fixed at $U_0 = 235$ V. The influence of pressure on the nonlinear dynamic behavior of the plasma system was studied using the tools such as waveforms, Fast Fourier Transform (FFT), and amplitude bifurcation diagrams. Fig.2 presents the temporal evolution

TABLE 1. Chemical reactions considered in the simulation.

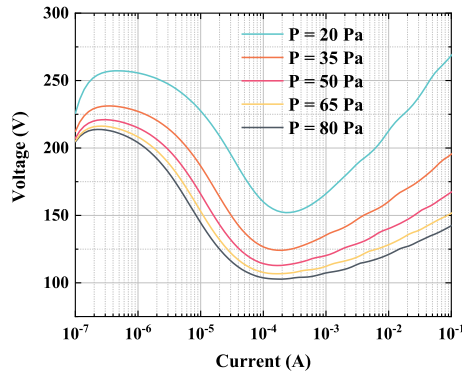| Reaction	Type	$\Delta E(eV)$	Constant
$e + Ar \rightarrow e + Ar$	Elastic collision	0	Cross section [34]
$e + Ar \rightarrow 2e + Ar^+$	Direct ionization	15.8	Cross section [34]
$e + Ar \rightarrow e + Ar_m$	Excitaion	11.5	Cross section [34]
$e + Ar_m \rightarrow e + Ar$	De-excitaion	-11.5	Cross section [34]
$e + Ar_m \rightarrow e + Ar^+$	Stepwise ionization	4.4	Cross section [34]
$Ar_m + Ar_m \rightarrow e + Ar + Ar^+$	Penning ionization	-	$6.2 \times 10^{-10} \mathrm{cm}^3 \mathrm{s}^{-1}$
$Ar_m + Ar \rightarrow Ar + Ar$	Metastable quenching	-	$3 \times 10^{-15} \mathrm{cm}^3 \mathrm{s}^{-1}$

FIGURE 1. The current-voltage characteristics (CVCs) at different pressures.

of the discharge voltage (first row), the discharge current (second row), the trajectory in the current-voltage phase space (third row) and the FFT of the discharge voltage (fourth row) at different pressures, respectively. As the pressure changes, a clear evolution in the dynamic behaviors of the system is observed. The results indicate that when the pressure p is below 27 Pa, the voltage is insufficient to initiate gas breakdown, resulting in the absence of temporal oscillations and the system operating in the stationary Townsend discharge regime. As the pressure is increased to slightly higher than 27 Pa, it can be seen from Fig. 2(a1) and Fig. 2(a2) that the Townsend discharge state is no longer maintained, resulting in an unstable discharge state with self-sustained oscillation. Meanwhile, a limit cycle attractor is present in the trajectory of the phase space (see Fig.2(a3)). The waveforms of the discharge voltage and current, along with the number of loops in the limit cycle, indicate that the discharge is in the period-1 oscillatory regime, where period-n represents that one period of the oscillation contains n pulses of different amplitudes. In the frequency domain, it can be seen from Fig.2(a4) that the FFT spectrum comprises a series of spikes, which correspond to the fundamental frequency $f_0 = 23.3$ kHz and its harmonics. As pressure increases, the discharge undergoes a series of period-doubling bifurcations and subsequently exhibits period-2 and period-4 oscillations (as illustrated in Fig.2(b1)~(b4) &(c1)~(c4)) [40], [41], [42], [43]. The more refined period-doubling bifurcation process is not depicted due to the impact of critical slowing down and limited numerical accuracy. Finally, the system will transition to a fully chaotic oscillatory regime

as shown in Fig.2(d1)~Fig.2(d4), which can be verified from the trajectory of the current-voltage phase space. The non-periodic nature can also be confirmed in the FFT spectrum, where continuous background noise is present alongside a series of spikes. When the pressure is increased further, the inverse process of mentioned above will occur: the system transitions from chaotic oscillations to periodic oscillation gradually. The plasma system then undergoes an inverse period-doubling bifurcation, followed by period-4 oscillation, period-2 oscillation, and finally period-1 oscillation (as shown in Fig.2(e1)~(e4) & (g1)~(g4)). When the pressure p is increased to about 37 Pa, the oscillations will disappear completely and the plasma system will transition to the stable glow discharge state.

To show the dynamic behavior evolution of the discharge system of the system more visually as the increasing of the pressure, the amplitude bifurcation diagram is plotted by recording the peak in the plasma voltage waveform at different pressure p in the oscillatory regime as shown in Fig.3, where the increment of the pressure Δp is 0.05 Pa. It can be seen from Fig.3 that the oscillatory regime can be generally divided into a period-doubling bifurcation stage and a corresponding inverse period-doubling bifurcation stage [44], [45], [46]. It is worth noting that the appearance of lower-order periodic states due to the inverse period-doubling bifurcation is related to the existence of two stationary states in parameter space (stationary Townsend discharge at low pressure and stationary glow discharge at high pressure), which is different from the one-dimensional unimodal mapping such as Logistic mapping. With the increase in pressure, the discharge system undergoes the following stages: stable Townsend discharge - occurrence of self-sustained periodic oscillation - period-doubling bifurcation - chaotic oscillation - inverse period-doubling bifurcation - periodic oscillation - stable glow discharge. Fig.4 shows the mean peak interval of the self-sustained oscillations at different pressures in the oscillatory regime. With the increasing pressure, the frequency of the self-sustained oscillations increases, attributed to the decrease in breakdown voltage and the shortened charging process of the RC external circuit.

Then the effect on the applied voltage on the dynamic behavior of the glow discharge is studied and the pressure is introduced as the second parameter and the dynamic behavior at different control parameters is shown. Fig.5(a) shows the single parameter amplitude bifurcation diagram of the discharge voltage with the applied voltage U_0 as
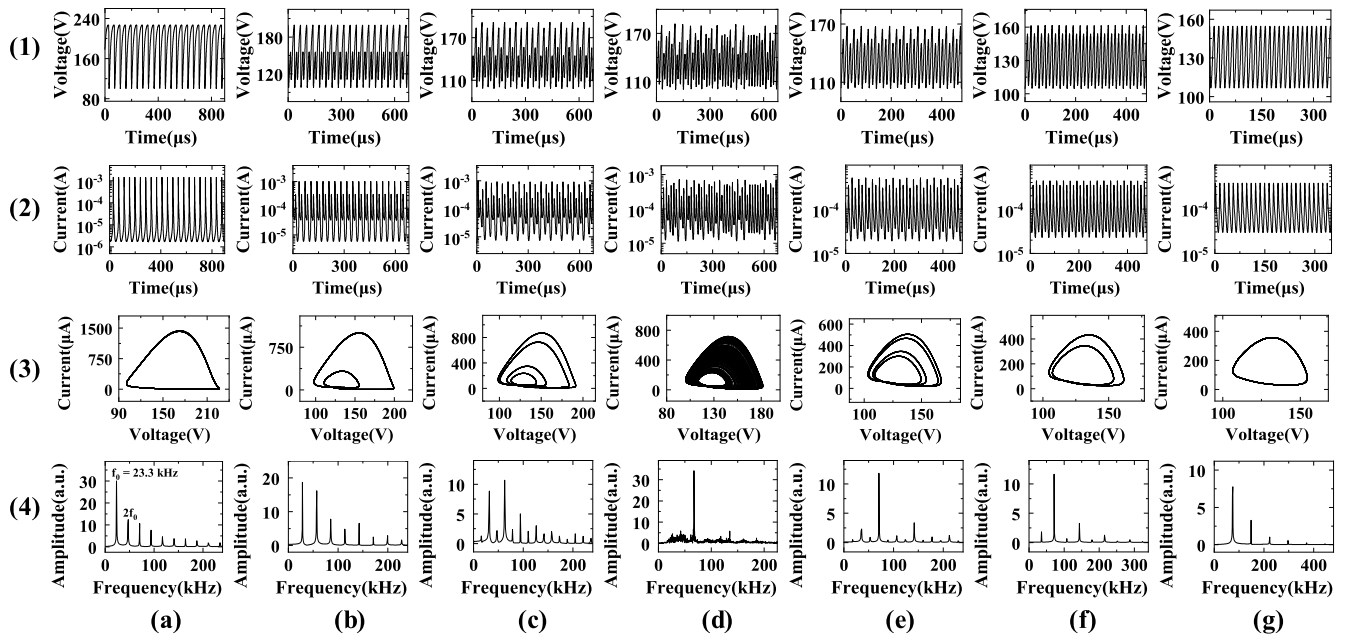
FIGURE 2. The evolution of the temporal oscillations of discharge voltage (first row) and discharge current (second row), the trajectory in the current-voltage phase space (third row) and the FFT spectrum (four row) at different pressures p = (a) 27 Pa, (b) 33 Pa, (c) 34.1 Pa, (d) 35 Pa, (e) 35.8 Pa, (f) 36.1 Pa, (g) 36.5 Pa.
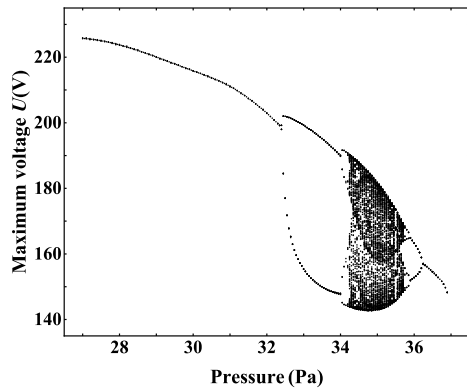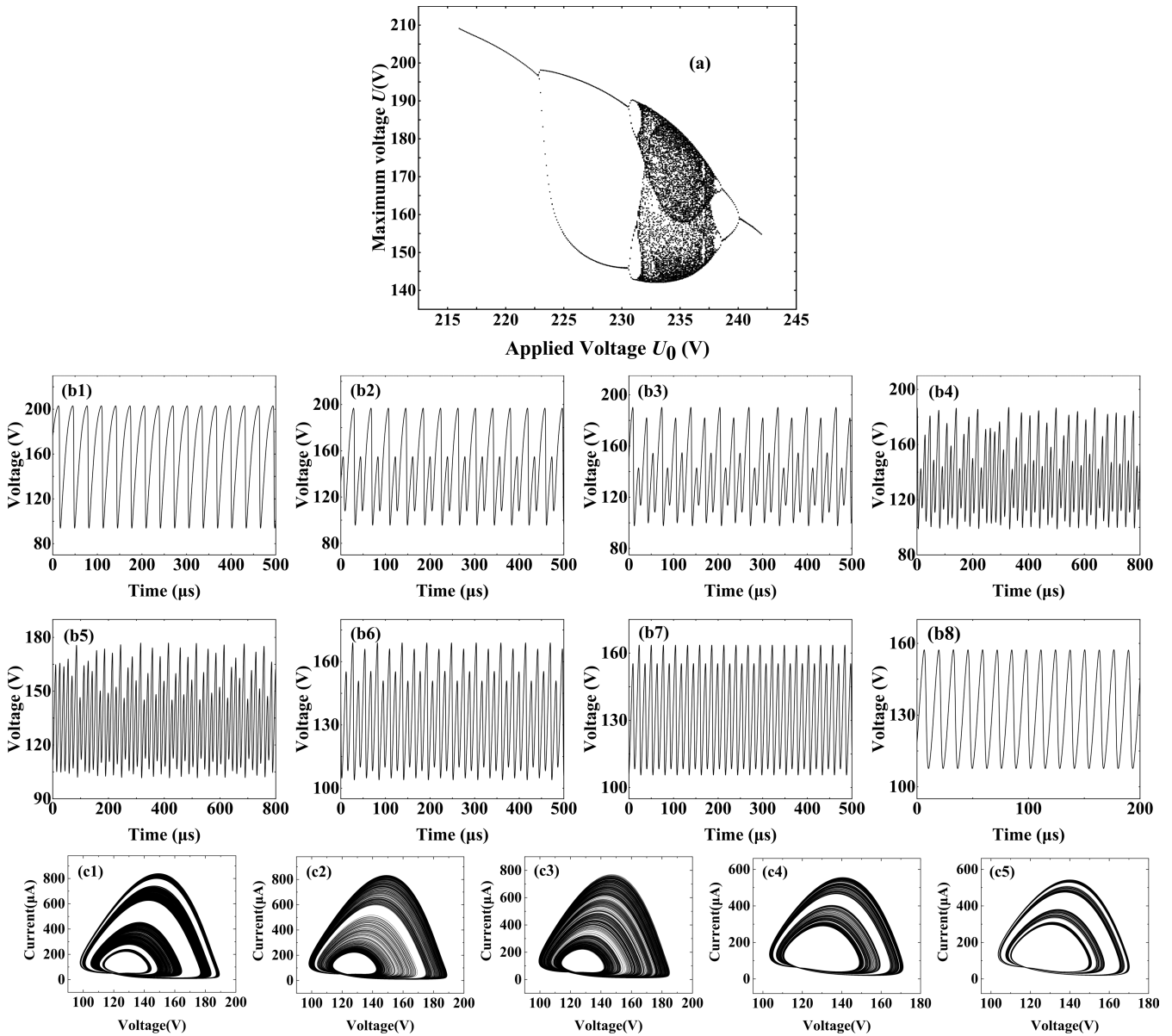

FIGURE 3. The amplitude bifurcation diagram, where the control parameter is selected as pressure and the interval is $\Delta p = 0.05$ Pa.
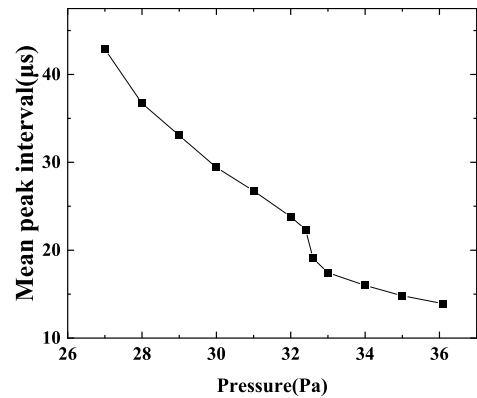
FIGURE 4. The mean peak interval of the self-sustained oscillations at different pressures.

the control parameter at an interval of 0.1 V for a fixed pressure of $p = 35$ Pa. It can be seen that Fig.5(a) and Fig.3 give a surprisingly comparable result. Fig.5(b) presents a series of the evolution of the discharge voltage at different U_0. It can be seen from Fig.5(a) & 5(b) that the system also successively undergoes the period-doubling bifurcation process and its inverse process and exhibits an order-chaos-order characteristic with the increasing of applied voltage. The result implies that the pressure and the applied voltage play a similar role in controlling the dynamic behavior of the system, which is due to the fact that the oscillatory regime is in the transition between the Townsend discharge and the glow discharge, and the ionization process is more likely to occur by both increasing the pressure and the applied voltage.

Fig.5(c) shows the strange attractors in the current-voltage phase space at different value of U_0 when the system enters chaos. As can be seen in Fig.5(c1), when the applied voltage $U_0 = 231.6$ V, the plasma system enters chaos through an inverse cascade process. The strange attractor of the system densely fills four band-like regions in the phase space, which is also referred to as the '4I' chaotic state in this case. With the increase in U_0, the chaotic bands merge, and the system transitions through the 4I state, 2I state, and finally becomes the 1I state (as shown in Fig.5(c1)~(c3)). The merging of chaotic bands can also be observed in the bifurcation diagram. With further increases in U_0, the chaotic bands gradually separate, as shown in Fig.5(c3)~(c5).
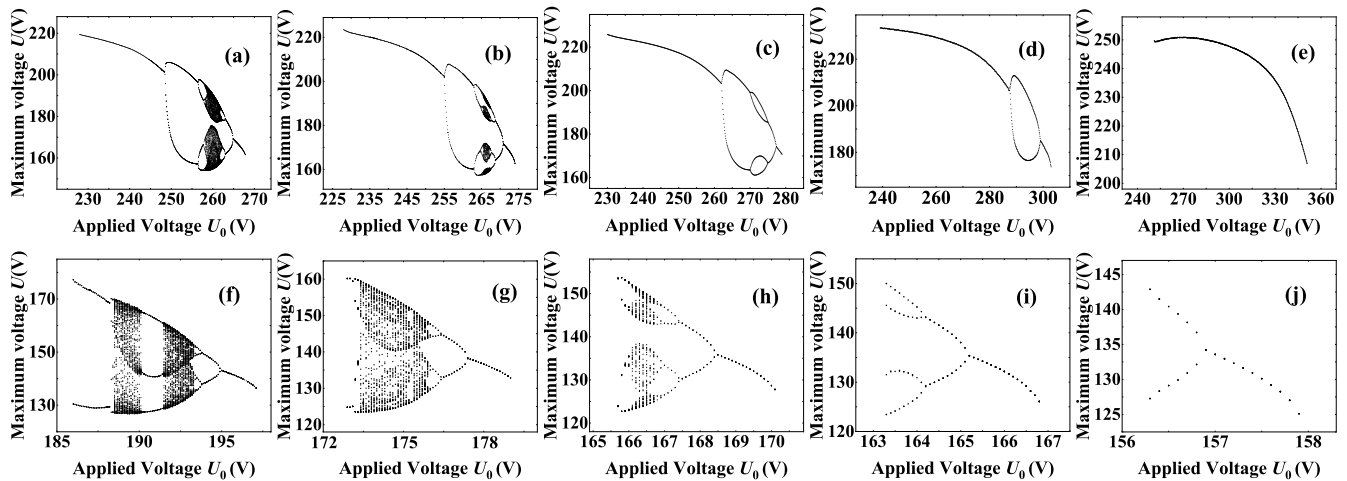
FIGURE 5. (a) Amplitude bifurcation diagram, where the control parameter is applied voltage and the pressure is fixed at 35 Pa. (b) The evolution of the temporal oscillations of discharge voltage for different applied voltages U_0 = (b1) 220 V, (b2) 225 V, (b3) 230.5 V, (b4) 234 V, (b5) 236.5 V, (b6) 238.3 V, (b7) 239.5 V, (b8) 242 V. (c) The trajectory of the current-voltage phase space for different applied voltages U_0 =(c1) 231.6 V, (c2) 231.8 V, (c3) 234 V, (c4) 237.8 V, (c5) 238 V.

The above analysis presents the period-doubling bifurcation route to chaos for the plasma system. However, it is important to note that the presence of chaos is related not only to the nonlinear nature of the system (which mainly refers to the form of the nonlinear equations in the simulation), but also to the choice of parameters in the equations. In fact, variations in pressure will cause the system to exhibit different dynamic behaviors when other discharge conditions are held constant, which is clearly demonstrated in the topological structure of the bifurcation diagram. Specifically, with varying pressure, a finite of "bubbles" is formed on some cross-sections of the two-parameter plane due to the finite period-doubling

bifurcation sequences and the corresponding remerging inverse bifurcation trees.

Then the bubbles structure is described in detail. Fig.6 shows the amplitude bifurcation diagrams of the discharge voltage for different pressures. Fig.6(a)∼(e) depict scenarios where the pressure is lower than 35 Pa, while Fig.6(f)∼(i) illustrate scenarios where the pressure is higher than 35 Pa. The bifurcation parameter is chosen as the applied voltage U_0, with a parameter interval of 0.1 V. First, the influence of the decrease in pressure on the system is analyzed. As can be seen from the Fig.6(a), when the pressure is decreased to 30 Pa, the plasma system still exhibits a period-doubling bifurcation and

FIGURE 6. Amplitude bifurcation diagram for p = (a) 30 Pa, (b) 29 Pa, (c) 28 Pa, (d) 25 Pa, (e) 20 Pa, (f) 50 Pa, (g) 60 Pa, (h) 67 Pa, (i) 70 Pa, (j) 80 Pa, where the control parameter is U_0.

an inverse bifurcation process as U_0 is changed. However, the difference from the case described above at $p = 35$ Pa is that as the pressure is decreased, the bifurcation structure of the system "shrinks" toward the center. This causes the chaotic bands to eventually merge not into the 1I state, but only into the 2I state. When the pressure decreases to 29 Pa, the bifurcation structure continues to shrink, causing the chaotic bands to merge into the 4I state, as depicted in Fig. 6(b). Furthermore, the rate of shrinkage accelerates gradually as the pressure decreases further. The process of shrinking the higher-order chaotic bands is not shown. When the pressure is further decreased to 28 Pa, it is not possible to observe chaotic oscillations over the whole range of the applied voltage in Fig.6(c). The period-doubling bifurcation will terminate in the period-4 oscillation mode and then the discharge will undergo the inverse period-doubling bifurcation and finally return to the period-1 oscillation. Even if the chaos can no longer be maintained, the shrinkage will continue. When the pressure is decreased to 25 Pa, it can be seen from Fig.6(d) that the period-4 mode in the bifurcation tree disappears, and the system transitions from the period-1 to the period-2 oscillation mode at about 287 V and returns to the period-1 oscillation mode by an inverse bifurcation at about 299 V. Besides, it is observed that as the pressure is decreased, the parameter range occupied by the forward bifurcation process gradually becomes wider compared to its inverse process. Finally, when the pressure is decreased to 20 Pa, the bifurcation process completely disappears in the whole applied voltage range and the discharge is in the period-1 oscillation mode throughout the unstable discharge regime.

On the contrary, the system undergoes a different change when the pressure is gradually increased, as depicted in Fig.6(f)~6(j). It can be seen from Fig.6(f) that when the pressure is increased to 50 Pa, the plasma system still maintains the transition of periodic oscillation-chaotic oscillation-periodic oscillation with the increase of U_0. However, the difference with the results in Fig.3 is that when U_0 is slightly

higher than the critical value of the stable Townsend discharge and the discharge evolves into the unstable oscillatory discharge state, the system directly transitions to the period-2 oscillation instead of the period-1 oscillation. In addition, it is worth noting that a period-3 window can be observed in the chaotic region which is caused by the saddle-node bifurcation [21]. The forward bifurcation process gradually disappears as the pressure increases, while the inverse bifurcation process remains basically unchanged (as shown in Fig.6(f)~6(h)). Meanwhile, the chaotic band separates at $p = 67$ Pa which is similar to that in Fig.6(a). When the pressure is further increased to 70 Pa, the chaotic phenomenon disappears completely, as shown in Fig.6(i). With the gradual increase in applied voltage, the plasma system transitions directly from the stable Townsend discharge mode to the period-4 oscillation mode. Subsequently, it changes to the period-1 discharge mode after undergoing two inverse bifurcation processes. The bifurcation structure is further simplified when the pressure is increased to 80 Pa, as shown in Fig.6(j). As the pressure continues to increase, only the period-1 oscillation mode remains in the bifurcation diagram, which is not shown here because the applied voltage range occupied by the instability region has become extremely small. It is clear from the results that the dynamics of the system are sensitive to pressure, even with slight changes, as the topology in the bifurcation diagram changes significantly. In conclusion, the dynamic behavior of the system becomes increasingly simpler with both the gradual decrease and increase of pressure.

IV. CONCLUSION
In this study, a two-dimensional, spatially dependent plasma fluid model based on the drift-diffusion approximation is developed and the external circuit is coupled as a boundary condition. The influence of the pressure on the dynamics of the low-pressure DC glow discharge which is working in the subnormal regime is studied. The discharge

dynamic behavior is characterized by the discharge voltage and current. The results show that the nonlinear dynamic behaviors are significantly influenced by the pressure, and a complete process of discharge mode evolution with pressure is obtained. As the pressure increases, the discharge undergoes a period-doubling bifurcation and an inverse bifurcation process and there is an order-chaos-order transition. In addition, the applied voltage is introducing as second control parameter. With varying pressure, it is found that a finite of "bubbles" is formed on some cross-sections of the two-parameter plane due to the finite period-doubling bifurcation sequences and the corresponding remerging inverse bifurcation trees. When the pressure is too high or low, chaos is not observed in the whole applied voltage range, instead only periodic oscillations occur.

From the perspective of low-temperature plasmas, current work demonstrates the influence of the pressure on the evolution of nonlinear discharge behavior and its bifurcation processes. It is significant in controlling discharge modes and providing guidance for actively choosing or avoiding chaotic discharges in practical applications, thereby optimizing self-pulsing discharges for various applications in the future. By adjusting discharge parameters, better control over discharge behavior can be achieved. In addition, the detailed dynamics studied in this work can provide a helpful reference for researchers interested in chaotic dynamics. As a simple and stable chaotic system, it also holds potential applications in fields such as chaotic synchronization, neural network and chaotic control. Through in-depth research into the dynamics of DC glow discharge systems, more effective chaotic control techniques and application strategies can be developed. The experimental validation and the exploration of the bifurcation mechanism based on linear stability analysis are objectives for future research.

DATA AVAILABILITY STATEMENT
The data that support the findings of this study are available upon reasonable request from the authors.

CONFLICT OF INTEREST
The authors declared that they have no conflicts of interest to this work.

REFERENCES
[1] A. Bogaerts, E. C. Neyts, O. Guaitella, and A. B. Murphy, "Foundations of plasma catalysis for environmental applications," *Plasma Sources Sci. Technol.*, vol. 31, no. 5, May 2022, Art. no. 053002.

[2] A. Bogaerts, A. Berthelot, S. Heijkers, S. Kolev, R. Snoeckx, S. Sun, G. Trenchev, K. Van Laer, and W. Wang, "CO$_2$ conversion by plasma technology: Insights from modeling the plasma chemistry and plasma reactor design," *Plasma Sources Sci. Technol.*, vol. 26, no. 6, May 2017, Art. no. 063001.

[3] Z. Chang, C. Wang, and G. Zhang, "Progress in degradation of volatile organic compounds based on low-temperature plasma technology," *Plasma Processes Polym.*, vol. 17, no. 4, Apr. 2020, Art. no. 1900131.

[4] M. Janda, V. Martišovitš, K. Hensel, L. Dvonč, and Z. Machala, "Measurement of the electron density in transient spark discharge," *Plasma Sources Sci. Technol.*, vol. 23, no. 6, Sep. 2014, Art. no. 065016.

[5] S. Chen, K. Li, and S. Nijdam, "Transition mechanism of negative DC corona modes in atmospheric air: From trichel pulses to pulseless glow," *Plasma Sources Sci. Technol.*, vol. 28, no. 5, May 2019, Art. no. 055017.

[6] A. Shaygani and K. Adamiak, "Numerical approaches in simulating trichel pulse characteristics in point-plane configuration," *J. Phys. D, Appl. Phys.*, vol. 56, no. 38, Sep. 2023, Art. no. 385202.

[7] Q. Xia, Y. Zhang, F. He, Y. Qin, Z. Jiang, and J. Ouyang, "Comparison between trichel pulse in negative corona and self-pulsing in other configurations," *Phys. Plasmas*, vol. 25, no. 2, Feb. 2018, Art. no. 23506.

[8] R. Cui, F. He, J. Miao, and J. Ouyang, "Experimental study on self-pulsing in flow-induced atmospheric pressure plasma jet," *Phys. Plasmas*, vol. 24, no. 10, Oct. 2017, Art. no. 103524.

[9] Z. Kovalová, M. Zahoran, A. Zahoranová, and Z. Machala, "Streptococ-cibiofilm decontamination on teeth by low-temperature air plasma of DC corona discharges," *J. Phys. D, Appl. Phys.*, vol. 47, no. 22, Jun. 2014, Art. no. 224014.

[10] M. Janda, K. Hensel, Z. Machala, and T. A. Field, "The influence of electric circuit parameters on NOx generation by transient spark discharge," *J. Phys. D, Appl. Phys.*, vol. 56, no. 48, Nov. 2023, Art. no. 485202.

[11] K. Kuč erová, Z. Machala, and K. Hensel, "Transient spark discharge generated in various N$_2$/O$_2$ gas mixtures: Reactive species in the gas and water and their antibacterial effects," *Plasma Chem. Plasma Process.*, vol. 40, no. 3, pp. 749–773, May 2020.

[12] H. Liu, J. Allen, D. Zheng, and F. Chen, "Recent development of respiratory rate measurement technologies," *Physiol. Meas.*, vol. 40, no. 7, Jul. 2019, Art. no. 07TR01.

[13] Z. Mokhtari, S. Holé, and J. Lewiner, "Smoke triggered corona discharge sensor," *J. Electrostat.*, vol. 71, no. 4, pp. 769–772, Aug. 2013.

[14] J. L. Walsh, F. Iza, N. B. Janson, and M. G. Kong, "Chaos in atmospheric-pressure plasma jets," *Plasma Sources Sci. Technol.*, vol. 21, no. 3, Jun. 2012, Art. no. 034008.

[15] P. Alex, M. Perumal, and S. K. Sinha, "Coexistence of chaotic and complexity dynamics of fluctuations with long-range temporal correlations under typical condition for formation of multiple anodic double layers in DC glow discharge plasma," *Nonlinear Dyn.*, vol. 101, no. 1, pp. 655–673, Jul. 2020.

[16] I. Rafatov, "Multiple stationary filamentary states in a planar DC-driven gas discharge-semiconductor system," *Phys. Plasmas*, vol. 23, no. 12, Dec. 2016, Art. no. 123506.

[17] I. Rafatov, "Numerical evidence of spontaneous division of dissipative solitons in a planar gas discharge–semiconductor system," *Phys. Plasmas*, vol. 26, no. 9, Sep. 2019, Art. no. 92105.

[18] H. Zhu, Z. Su, and Y. Dong, "Experimental studies on striations in helium glow discharge," *Appl. Phys. Lett.*, vol. 111, no. 5, Jul. 2017, Art. no. 54104.

[19] V. I. Kolobov and R. R. Arslanbekov, "Ionization waves in low-current DC discharges in noble gases obtained with a hybrid kinetic-fluid model," *Phys. Rev. E, Stat. Phys. Plasmas Fluids Relat. Interdiscip. Top.*, vol. 106, no. 6, Dec. 2022, Art. no. 065206.

[20] P. Y. Cheung and A. Y. Wong, "Chaotic behavior and period doubling in plasmas," *Phys. Rev. Lett.*, vol. 59, no. 5, pp. 551–554, Aug. 1987.

[21] J. Qin, L. Wang, D. P. Yuan, P. Gao, and B. Z. Zhang, "Chaos and bifurcations in periodic windows observed in plasmas," *Phys. Rev. Lett.*, vol. 63, no. 2, pp. 163–166, Jul. 1989.

[22] I. Rafatov and C. Yesil, "Transition from homogeneous stationary to oscillating state in planar gas discharge–semiconductor system in nitrogen: Effect of fluid modelling approach," *Phys. Plasmas*, vol. 25, no. 8, Aug. 2018, Art. no. 82107.

[23] D. Mansuroglu and I. U. Uzun-Kaymak, "Experimental analysis on the nonlinear behavior of DC barrier discharge plasmas," *Plasma Sci. Technol.*, vol. 19, no. 1, Jan. 2017, Art. no. 015401.

[24] F.-C. Liu, W. Yan, and D.-Z. Wang, "Phenomena of oscillations in atmospheric pressure direct current glow discharges," *Phys. Plasmas*, vol. 20, no. 12, Dec. 2013, Art. no. 122116.

[25] E. Pugliese, R. Meucci, S. Euzzor, J. G. Freire, and J. A. C. Gallas, "Complex dynamics of a DC glow discharge tube: Experimental modeling and stability diagrams," *Sci. Rep.*, vol. 5, no. 1, p. 8447, Feb. 2015.

[26] Y. Hong, W. Ning, D. Dai, and Y. Zhang, "Influence of air impurities on the transition from a symmetric discharge to an asymmetric discharge in an atmospheric pressure helium diffuse dielectric barrier discharge," *Phys. Plasmas*, vol. 27, no. 5, May 2020, Art. no. 53510.

[27] Y. Hong and Y. Han, "Nonlinear dynamics of atmospheric-pressure helium diffuse dielectric barrier discharge in a two-parameter plane," *IEEE Trans. Plasma Sci.*, vol. 49, no. 11, pp. 3566–3575, Nov. 2021.

[28] Y. Fu, J. P. Verboncoeur, A. J. Christlieb, and X. Wang, "Transition characteristics of low-pressure discharges in a hollow cathode," *Phys. Plasmas*, vol. 24, no. 8, Aug. 2017, Art. no. 83516.

[29] M. A. Lieberman and A. J. Lichtenberg, "Principles of plasma discharges and materials processing," *MRS Bull.*, vol. 30, no. 12, pp. 899–901, 1994.

[30] Y. P. Raizer and J. E. Allen, *Gas Discharge Physics*, vol. 2. Berlin, Germany: Springer, 1997.

[31] E. A. Bogdanov, S. F. Adams, V. I. Demidov, A. A. Kudryavtsev, and J. M. Williamson, "Influence of the transverse dimension on the structure and properties of DC glow discharges," *Phys. Plasmas*, vol. 17, no. 10, Oct. 2010, Art. no. 103502.

[32] I. Rafatov, E. Bogdanov, and A. Kudryavtsev, "On the accuracy and reliability of different fluid models of the direct current glow discharge," *Phys. Plasmas*, vol. 19, no. 3, 2012, Art. no. 33502.

[33] I. Rafatov, E. Bogdanov, and A. Kudryavtsev, "Account of nonlocal ionization by fast electrons in the fluid models of a direct current glow discharge," *Phys. Plasmas*, vol. 19, no. 9, 2012, Art. no. 93503.

[34] *Phelps Database*. Accessed: Mar. 2024. [Online]. Available: www.lxcat.net/Phelps

[35] R. R. Arslanbekov and V. I. Kolobov, "Two-dimensional simulations of the transition from Townsend to glow discharge and subnormal oscillations," *J. Phys. D, Appl. Phys.*, vol. 36, no. 23, pp. 2986–2994, Dec. 2003.

[36] H. Jing and S. He, "Spatio-temporal characteristics of self-pulse in hollow cathode discharge," *Phys. Plasmas*, vol. 22, no. 2, Feb. 2015, Art. no. 22106.

[37] M. Mahdizadeh, G. Foroutan, and V. Foroutan, "A simulation study of the self-pulsing regime of a micro hollow cathode discharge in helium using a zero-dimensional model," *Phys. Scripta*, vol. 96, no. 12, Dec. 2021, Art. no. 125602.

[38] Y. P. Raizer and M. Mokrov, "Physical mechanisms of self-organization and formation of current patterns in gas discharges of the Townsend and glow types," *Phys. Plasmas*, vol. 20, no. 10, 2013, Art. no. 101604.

[39] I. Rafatov, "Three-dimensional numerical modelling of temporal and spatial pattern formation in a DC-driven gas discharge-semiconductor system," *Plasma Sources Sci. Technol.*, vol. 25, no. 6, Oct. 2016, Art. no. 065014.

[40] M. D. Vijayakumar, H. Natiq, M. I. Tametang Meli, G. D. Leutcho, and Z. T. Njitacke, "Hamiltonian energy computation of a novel memristive mega-stable oscillator (MMO) with dissipative, conservative and repelled dynamics," *Chaos, Solitons Fractals*, vol. 155, Feb. 2022, Art. no. 111765.

[41] G. D. Leutcho, L. Woodward, and F. Blanchard, "Nonlinear dynamics of a single-gap terahertz split-ring resonator under electromagnetic radiation," *Chaos, Interdiscipl. J. Nonlinear Sci.*, vol. 33, no. 10, Oct. 2023, Art. no. 103131.

[42] G. D. Leutcho, T. F. Fozin, A. N. Negou, Z. T. Njitacke, V.-T. Pham, J. Kengne, S. Jafari, and C. Aguilar-Ibanez, "A novel megastable Hamiltonian system with infinite hyperbolic and nonhyperbolic equilibria," *Complexity*, vol. 2020, pp. 1–12, Sep. 2020.

[43] B. Ramakrishnan, H. Natiq, K. Rajagopal, S. Jafari, P. L. Ndukum, and G. D. Leutcho, "Approximate symmetry memristive mega-stable oscillator with attractor growing and its Hamilton energy balance," *Eur. Phys. J. Plus*, vol. 137, no. 5, pp. 1–10, May 2022.

[44] X. Han, Z. Chen, and Q. Bi, "Inverse period-doubling bifurcations determine complex structure of bursting in a one-dimensional non-autonomous map," *Chaos, Interdiscipl. J. Nonlinear Sci.*, vol. 26, no. 2, Feb. 2016, Art. no. 23117.

[45] V. Van Huynh, A. J. M. Khalaf, A. Alsaedi, T. Hayat, and H. R. Abdolmohammadi, "A new memristive chaotic flow with a line of equilibria," *Eur. Phys. J. Special Topics*, vol. 228, no. 10, pp. 2339–2349, Oct. 2019.

[46] L. F. Olsen and A. Lunding, "Chaos in the peroxidase–oxidase oscillator," *Chaos, Interdiscipl. J. Nonlinear Sci.*, vol. 31, no. 1, Jan. 2021, Art. no. 13119.

XITONG ZHAO is currently pursuing the bachelor's degree with Shanghai University, China. She has published one article in an academic journal. Her research interests include data structures and algorithms, nonlinear phenomena in media, and physical modeling and simulation.

• • •